

# The Hippo Pathway Maintains the Equatorial Division Plane in the Ciliate *Tetrahymena*

Yu-Yang Jiang,\* Wolfgang Maier,<sup>†</sup> Ralf Baumeister,<sup>†\*</sup> Gregory Minevich,<sup>§</sup> Ewa Joachimiak,\*\* Zheng Ruan,\*\* Natarajan Kannan,\*\*<sup>††</sup> Diamond Clarke,\* Joseph Frankel,<sup>§§</sup> and Jacek Gaertig\*<sup>1</sup>

\*Department of Cellular Biology, <sup>††</sup>Institute of Bioinformatics, and <sup>†††</sup>Department of Biochemistry and Molecular Biology, University of Georgia, Athens, Georgia 30602, <sup>†</sup>Bio3/Bioinformatics and Molecular Genetics (Faculty of Biology) and ZMBZ (Faculty of Medicine), <sup>‡</sup>Centre for Biological Signalling Studies (BIOSS), Albert-Ludwigs-University of Freiburg, 79104 Germany, <sup>§</sup>Department of Biochemistry and Molecular Biophysics, Columbia University Medical Center, New York, New York 10032, \*\*Laboratory of Cytoskeleton and Cilia Biology, Department of Cell Biology, Nencki Institute of Experimental Biology of Polish Academy of Sciences, 02-093 Warsaw, Poland, and <sup>§§</sup>Department of Biology, University of Iowa, Iowa City, Iowa 52242

**ABSTRACT** The mechanisms that govern pattern formation within the cell are poorly understood. Ciliates carry on their surface an elaborate pattern of cortical organelles that are arranged along the anteroposterior and circumferential axes by largely unknown mechanisms. Ciliates divide by tandem duplication: the cortex of the predivision cell is remodeled into two similarly sized and complete daughters. In the conditional *cdal-1* mutant of *Tetrahymena thermophila*, the division plane migrates from its initially correct equatorial position toward the cell's anterior, resulting in unequal cell division, and defects in nuclear divisions and cytokinesis. We used comparative whole genome sequencing to identify the cause of *cdal-1* as a mutation in a Hippo/Mst kinase. Cdal is a cortical protein with a cell cycle-dependent, highly polarized localization. Early in cell division, Cdal marks the anterior half of the cell, and later concentrates at the posterior end of the emerging anterior daughter. Despite the strong association of Cdal with the new posterior cell end, the *cdal-1* mutation does not affect the patterning of the new posterior cortical organelles. We conclude that, in *Tetrahymena*, the Hippo pathway maintains an equatorial position of the fission zone, and, by this activity, specifies the relative dimensions of the anterior and posterior daughter cell.

**KEYWORDS** Hippo; *Tetrahymena*; cytokinesis; ciliate; polarity

CILIALES are among the most structurally complex cell types known, due to their nuclear dualism and the intricate organization of their surface. Ciliates have two structurally and functionally distinct nuclei that operate in one cytoplasm: the germline micronucleus that undergoes mitosis (or meiosis), and the somatic macronucleus that divides by amitosis—a unique mode of nuclear division that does not involve chromatin condensation or a bipolar spindle formation (reviewed in Ruehle *et al.* 2016). During the vegetative cell cycle, these two nuclei divide at different times, with the mitosis of the micronucleus preceding the amitosis of the macronucleus (Figure 1). In addition, during cell division,

ciliates duplicate the cortex, to produce a tandem of daughter cells (reviewed in Wloga and Frankel 2012).

The tandem duplication of the cortical pattern has to be precisely coordinated with cytokinesis in time and space. The cortical regions immediately anterior and posterior to the fission zone undergo vastly different morphogenetic routines, to develop new cortical ends (see Figure 1). The division plane establishes an asymmetry in the cell cortex that is manifested by different organelles that appear on each side of the cleavage furrow: the new cytoproct and contractile vacuole pores form above, and the new cell apex emerges below the cleavage furrow, respectively (Frankel *et al.* 1981; Jerka-Dziadosz 1981; Numata *et al.* 1995; Kaczanowska *et al.* 1999; Cole *et al.* 2008). The first sign of cell division is the formation of the oral primordium (a developing new oral apparatus) within the confines of the posterior subcell (the term “subcell” describes a half of the dividing cell that will give rise to either the anterior or the posterior daughter). Next, in the region directly anterior to the oral primordium,

Copyright © 2017 by the Genetics Society of America

doi: <https://doi.org/10.1534/genetics.117.200766>

Manuscript received February 1, 2017; accepted for publication March 29, 2017; published Early Online April 14, 2017.

<sup>1</sup>Corresponding author: Department of Cellular Biology, University of Georgia, 724 Biological Sciences Bldg., Athens, GA 30602. E-mail: [jgaertig@uga.edu](mailto:jgaertig@uga.edu)

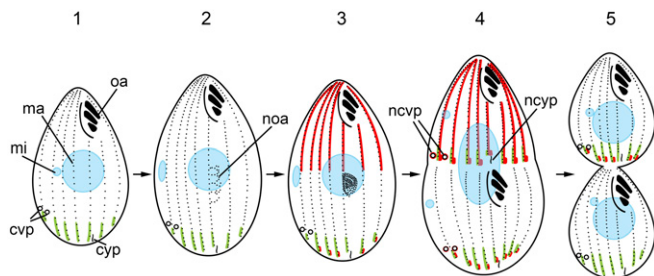


**Figure 1** A diagram that presents the cortical and nuclear stages of cell division by tandem duplication in *Tetrahymena*. The green and red lines indicate the patterns of Hippo signaling components: CdaI (red, this study) and Mob1 (green, based on Tavares *et al.* 2012). mi, micronucleus; ma, macronucleus; oa, oral apparatus; noa, new oral apparatus (primordium); cvp, contractile vacuole pore; ncvp, new contractile vacuole pore; cyp, cytoproct; ncyp, new cytoproct. The stage designations are novel to this paper and the numbers do not correspond to the earlier named stages of oral development (Nelsen *et al.* 1981).

the ciliary rows become interrupted by a gap, the “cortical subdivision,” which demarcates the emerging daughters. At about the same time, the new cortical ends start to differentiate, and this is manifested by the appearance of the new contractile vacuole pores, and the new cytoproct at the posterior end of the anterior daughter. How the cortical events of tandem duplication are accomplished, and, specifically, how they are coordinated with cytokinesis, is not known.

A set of potentially informative conditional *Tetrahymena* mutants that are affected in cell division have been generated by random chemical mutagenesis, but most of the genes responsible remain unknown (Frankel *et al.* 1976, 1977; Frankel 2008). Recently, comparative whole genome sequencing has been used for identification of causative mutations in *Tetrahymena*, and in another ciliate, *Paramecium* (Galati *et al.* 2014; Marker *et al.* 2014; Kontur *et al.* 2016). An important breakthrough was the identification of the first mutation that alters the cortical pattern in *Tetrahymena*, *disA-1* (Galati *et al.* 2014). Here, we use whole genome sequencing to identify the causative mutation for *cdaI-1*, a temperature-sensitive mutation that results in unequal cell division (Frankel 2008), in a homolog of Hippo/Mst kinases, a conserved component of Hippo signaling (reviewed in Yu *et al.* 2015). *cdaI-1* phenocopies a loss-of-function of the conserved substrate of Hippo/Mst kinases, Mob1 (Tavares *et al.* 2012). We conclude that ciliates utilize the Hippo pathway for achieving equatorial division. Our observations also indicate that ciliates must have additional yet unknown mechanisms, independent of CdaI, for setting up the anteroposterior and circumferential axes.

## Materials and Methods

### *Tetrahymena* strains

To identify the causal mutation for *cdaI-1*, we used the strain IA237 *cdaI-1/cdaI-1* (*cdaI-1*, II). For the outcross, we used the heterokaryon strain CU427 *chx1-1/chx1-1* (*CHX1*, *cy-s*, mt VI). The CU428 strain *mpr1-1/mpr1-1* (*MPR1*, *mp-s*, mt VII) was

used as a wild type for comparisons of phenotypes. The B\*VII strain was used for the self-cross. The expression of CdaI-GFP transgene was performed in CU428 as well as in the background of *elo1-1*, a mutation that shifts the division plane posteriorly, using strain IA388 *elo1-1/elo1-1* (*elo1-1*; I). All strains were obtained from the *Tetrahymena* Stock Center, Cornell University (Ithaca, NY). Cells were grown in SPP medium (Gorovsky 1973) with antibiotics (SPPA; Gaertig *et al.* 2013) at 28–30° (standard temperature that is permissive for *cdaI-1*) or 39–40° (restrictive temperature for *cdaI-1*).

### Crosses and preparation of pools for next generation sequencing

Standard methods for crosses and analyses of progeny were used (Orias *et al.* 2000) unless mentioned otherwise. To identify the causative mutation for *cdaI-1*, we used a modified “bulked segregant” approach (Michelmore *et al.* 1991; Birkeland *et al.* 2010) that includes a self-cross. The IA237 *cdaI-1* mutant strain was crossed to the heterokaryon CU427, and F1 heterozygotes were recovered based on cycloheximide resistance (*cy-r*, 15  $\mu$ g/ml). Several *cy-r* F1 heterozygotes were cloned and grown for >60 generations for sexual maturation and macronuclear assortment to cycloheximide sensitivity. A single fertile *cy-s* F1 was used for a self-cross to B\*VII to produce the “short-circuit genomic exclusion (SCGE)” progeny (Bruns *et al.* 1976) as follows. The *CDAI/cdaI-1* *cy-s* F1 and B\*VII cells were grown to  $\sim 2\text{--}3 \times 10^5$  cell/ml in 5 ml of SPPA at 30°. The cells were washed, suspended in 5 ml of 10 mM Tris-HCl pH 7.5 and starved for 18 hr at 30°. The starved F1 and B\*VII cells (400  $\mu$ l each) were mixed in a single well of a 24-well microtiter plate, and allowed to mate at 30° for 6.5 hr. The mating cells were diluted to 10 ml with SPPA, and plated on a 96-well microtiter plate at 50  $\mu$ l/well. The plates were incubated for 18 hr at 30°, and 50  $\mu$ l of SPPA with 30  $\mu$ g/ml of *cy* was added to each well. After 2 days of selection, 192 single *cy-r* F2 cells (each from a different well to ensure that they come from independent meioses) were isolated into drops of SPPA on Petri dishes. The F2 *cy-r* clones were replicated onto 96-well microtiter plates with 100  $\mu$ l/well of SPPA, incubated overnight at 39°, and scored for either a wild-type or *cdaI-1* phenotype. Thirty-six wild-type and 36 separate *cdaI-1* F2 clones were pooled. The clonal pools were grown overnight in 25 ml of SPPA, washed and suspended in 60 mM Tris-HCl pH 7.5 [this unusual concentration of Tris-HCl is used to block pairing (Bruns and Brussard 1974)], and starved for 2 days at the room temperature. Total genomic DNAs were extracted from the two F2 pools with the urea method as described (Dave *et al.* 2009).

### Whole genome sequencing and causative variant identification using the macronuclear reference genome

The pool DNAs were used to prepare libraries using Illumina Truseq adapters and sequenced by the Illumina MiSeq instrument to generate paired-end reads of 300 bp with 30 $\times$  coverage. The following sequence analyses were performed using the Galaxy web-based platform (Afgan *et al.* 2016)

(<https://usegalaxy.org>). The sequence reads were aligned to the macronuclear reference genome (June 2014 version, GenBank assembly accession GCA\_000189635.1) (Eisen *et al.* 2006). FASTQ Quality Trimmer was used to remove ends of reads with aggregate quality score <20 (Blankenberg *et al.* 2010). The reads were aligned to the macronuclear reference genome using BWA-MEM (Li and Durbin 2009), and realigned around indels using GATK (McKenna *et al.* 2010; DePristo *et al.* 2011). PCR duplicates were removed using Picard (<http://broadinstitute.github.io/picard>). Homozygous variants were called using GATK Unified Genotyper. Next we used the GATK Select Variants tool to remove variants from the mutant pool that were also present in: (1) the sister F2 wild-type pool and (2) six pools that originated from independent projects using non-*cdal-1* backgrounds and the same genetic scheme (our unpublished data). The remaining variants were filtered for the types of mutations that are commonly induced by nitrosoguanidine (Ohnishi *et al.* 2008) using SnpSift (Cingolani *et al.* 2012) with the expression: ((REF = 'G') & (ALT = 'A')) | ((REF = 'C') & (ALT = 'T')) | ((REF = 'T') & (ALT = 'C')) | ((REF = 'A') & (ALT = 'G')). The remaining candidate variants were annotated using SnpEff (Cingolani *et al.* 2012). Sequence reads containing candidate variants were inspected manually in the IGV genome browser (Robinson *et al.* 2011; Thorvaldsdottir *et al.* 2013).

#### Identification of the causative micronuclear chromosomal region by allelic composition contrast analysis

To map the location of the causative variant on the micronuclear genome, we used a customized version of MiModD (<https://sourceforge.net/projects/mimodd/>) as follows. We aligned the mutant and wild-type pool reads to the micronuclear genome assembly of *T. thermophila*, strain SB210 (GenBank assembly accession GCA\_000261185.1) (Hamilton *et al.* 2016), and performed joint variant calling of both pools against the reference, keeping all variants that appeared at least heterozygous in one of the two samples. A linkage score quantifying the difference in the allelic composition between the mutant and the wild-type pool was then computed at each variant site. When plotted against genomic coordinates, this score is expected to peak near the location of the causative variant.

#### Rescue

A fragment of *THERM\_00971920* was amplified from the wild-type genomic DNA (CU428 strain) using primers: 5'-TGTTACTGCAACACCAGA-3' and 5'-GGTCAAGGCTCATATGGAA-3', and introduced by biolistic bombardment (Bruns and Cassidy-Hanley 2000) into starved *cdal-1* IA237. Cells were grown on the 96-well plates at the restrictive temperature, and inspected for the appearance of wild-type cells. Mock-transformed cells were used as a negative control.

#### Imaging of Cdal-GFP and analyses of Cdal mutants

To determine the localization of CdaI, a GFP sequence was added to the 3' end of the ORF predicted for *THERM\_00971920*

(*CDAI*), using a linked *neo5* marker (Busch *et al.* 2010). The macronuclear assortment of the tagged allele was promoted by growing cells in increasing concentrations of paromomycin starting at 120  $\mu\text{g/ml}$ . The GFP tagging of CdaI was done in the wild-type background (CU428), and in the *elo1-1* mutant (IA388). To evaluate the morphological phenotypes, cells were labeled by immunofluorescence with simultaneous fixation and permeabilization (Gaertig *et al.* 2013), using 20H5 monoclonal anti-centrin antibody (Millipore) (Sanders and Salisbury 1994), or 6-11 B-1 anti-acetyl-K40  $\alpha$ -tubulin antibody (Sigma-Aldrich) (Piperno and Fuller 1985) or polyclonal anti-GFP (Rockland) antibodies, followed by secondary antibodies coupled to either CY3 or fluorescein (Rockland). DNA was stained using DAPI. The imaging was done on a Zeiss LSM 710 confocal fluorescence microscope.

#### Data availability

The authors state that all data necessary for confirming the conclusions presented in the article are represented fully within the article.

## Results

### Cortical and nuclear defects in the *cdal-1* Tetrahymena mutant

The *cdal-1* *Tetrahymena* clone was isolated in a screen for cell division mutants, which involved exposure to nitrosoguanidine (Frankel *et al.* 1976) followed by cytogamy to bring mutations to expression (Orias *et al.* 1979). *cdal-1* is a temperature-sensitive, recessive mutation. The *cdal-1* cells appear morphologically normal when grown at 28–30° and undergo a severe anterior displacement of the division furrow at 39–40° (Frankel 2008). We used anti-centrin antibodies (Sanders and Salisbury 1994) to evaluate the cortical organization in the wild type and *cdal-1* mutants. The anti-centrin antibodies label the basal bodies of both the locomotory ciliary rows that span the entire cell length, and the four sets of short ciliary rows that are parts of the oral apparatus. In the wild-type cells or in the *cdal-1* cells grown at the permissive temperature, the first sign of cell division is the appearance of the new oral apparatus (oral primordium), as a cluster of basal bodies that form adjacent to the right postoral ciliary row at a sub-medial location (Figure 1, stage 2 and Figure 2A). Next, the basal bodies of the oral primordium organize into subsets that give rise to the oral rows (Figure 1, stage 3 and Figure 2B). Coincident with the completed differentiation of these structures, the longitudinal ciliary rows develop the “cortical subdivision,” a gap that circumscribes the cell at a medial location (Figure 1, stage 4 and Figure 2C). The subsequent cytokinesis occurs within the cortical subdivision (Figure 1, stage 5 and Figure 2D). The micronucleus undergoes closed mitosis around the time of the initiation of cortical subdivision (Figure 1, stages 3 and 4 and Figure 2C), while the macronucleus divides by amitosis at the time of constriction of the contractile ring (Figure 1, stage 4 and 5 and Figure 2D).

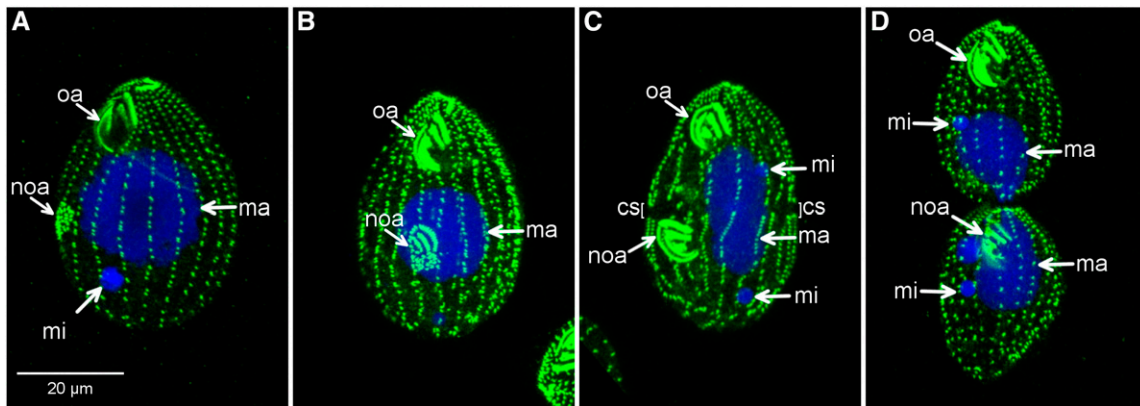


**Figure 2** Cortical pattern and nuclei during cell division in wild-type *Tetrahymena* grown at 39°. The cells were labeled with anti-centrin 20H5 antibodies (green) and DAPI (blue). (A, B) Early stages of cell division. A new oral primordium develops [more advanced in (B)], but there is no sign of cortical subdivision yet. (C) A cell with a well-developed cortical subdivision, but before cytokinesis. The micronucleus has already completed its mitosis and the two progeny micronuclei are present. The macronucleus is elongated, in an early stage of amitosis. (D) A cell in a late stage of cytokinesis, the macronucleus has divided by amitosis. oa, oral apparatus; noa, new oral apparatus; mi, micronucleus, ma, macronucleus; cs, cortical subdivision.

At the restrictive temperature, the *cdal-1* mutants developed an oral primordium at a correct medial and circumferential position (Figure 3, A and B). However, at the later stage, the new oral apparatus was seen immediately posterior to the old oral apparatus (Figure 3C), most likely due to its anterior translocation. The basal bodies of the two postoral rows that in wild type are positioned between the new and the old oral apparatus, in the mutants shorten or completely disappear (Figure 3C and data not shown). Consistently with the anterior shift of the new OA, the cortical subdivision forms at an excessively anterior position but still in the space between the two OAs (Figure 3C). The cortical subdivision and the subsequent cytokinesis are delayed, but eventually subcells differentiate, except that they are unequal in size (Figure 3, D and F). Often, the smaller anterior subcell tilts resulting in a “hammerhead” shape of the dividing cell (Figure 3, D and F). The tilting could be a consequence of an incomplete or asymmetrically delayed cortical subdivision; often in the same hammerhead, some of the ciliary rows are subdivided, while other rows maintain continuity between the anterior and posterior subcell, which could produce an asymmetry in the growth of the cortex (Figure 3, D and F). The progression of the mutant phenotype outlined above is supported by the quantification of the morphological phenotypes at 3 and 6 hr at the restrictive temperature (Figure 3H). In some *cdal-1* cells, cytokinesis, while delayed, runs to completion, generating an excessively large posterior daughter (Figure 3, D and F), and an excessively small anterior daughter (Figure 3E). In other mutant cells, cytokinesis fails, and the posterior cell enters a new cell cycle, producing a second generation anterior subcell (Figure 3G). The mitotic division of the micronucleus takes place in the majority of mutant cells, but often the anterior subcell does not receive a progeny micronucleus (Figure 3, G and I). In contrast, in most mutants, the macronucleus fails to divide and remains in the posterior subcell (Figure 3, D, E, G, and I). Consequently,

when the abscission is successful, often the anterior daughter lacks a macronucleus or lacks the nuclei altogether (Figure 3, E, G, and I and Figure 9G).

#### Identification of the causal mutation of *cdal-1* by whole genome sequencing

We used a modified “bulked segregant” approach (Michelmore *et al.* 1991; Birkeland *et al.* 2010) that includes a self-cross, similar to what was used with *Paramecium tetraurelia* (Marker *et al.* 2014). The principle is to subject an F1 heterozygote to a number of independent meioses, and to identify a mutation that among the F2 progeny strictly cosegregates with the mutant phenotype. We performed an SCGE self-cross by mating an F1 to B\*VII (a strain that lacks a functional micronucleus), with the intention of producing progeny that are homozygous postmeiotic derivatives of the F1 genome (Bruns *et al.* 1976). The F2s were expected to display a 1:1 segregation of the mutant vs. wild-type phenotypes. Among a total of 100 F2 clones picked, at the restrictive temperature, 63 were wild type and 37 were *cdal-1* (1.7:1 ratio). The apparent deviation of the segregation pattern from the expected 1:1 ratio is explained by our subsequent observation that the SCGE self-cross, in addition to expected homozygotes apparently also produced some F2 heterozygotes (see below). We prepared pools of 36 F2 clones that were phenotypically either wild type or *cdal-1*. Both pools were subjected to whole genome sequencing and variant identification.

We aligned the mutant and wild-type pool sequence reads to the macronuclear reference genome (Eisen *et al.* 2006). Following variant calling, we narrowed down the list of candidate mutations through stepwise filtering and subtraction as follows (Figure 4A). We detected 3444 and 3566 variants that were prominent enough in the *cdal-1* and the wild-type pool, respectively, and 1009 of these were unique to *cdal-1* and were analyzed further (Figure 4A). We subtracted those mutant pool variants that were also detected in six pools

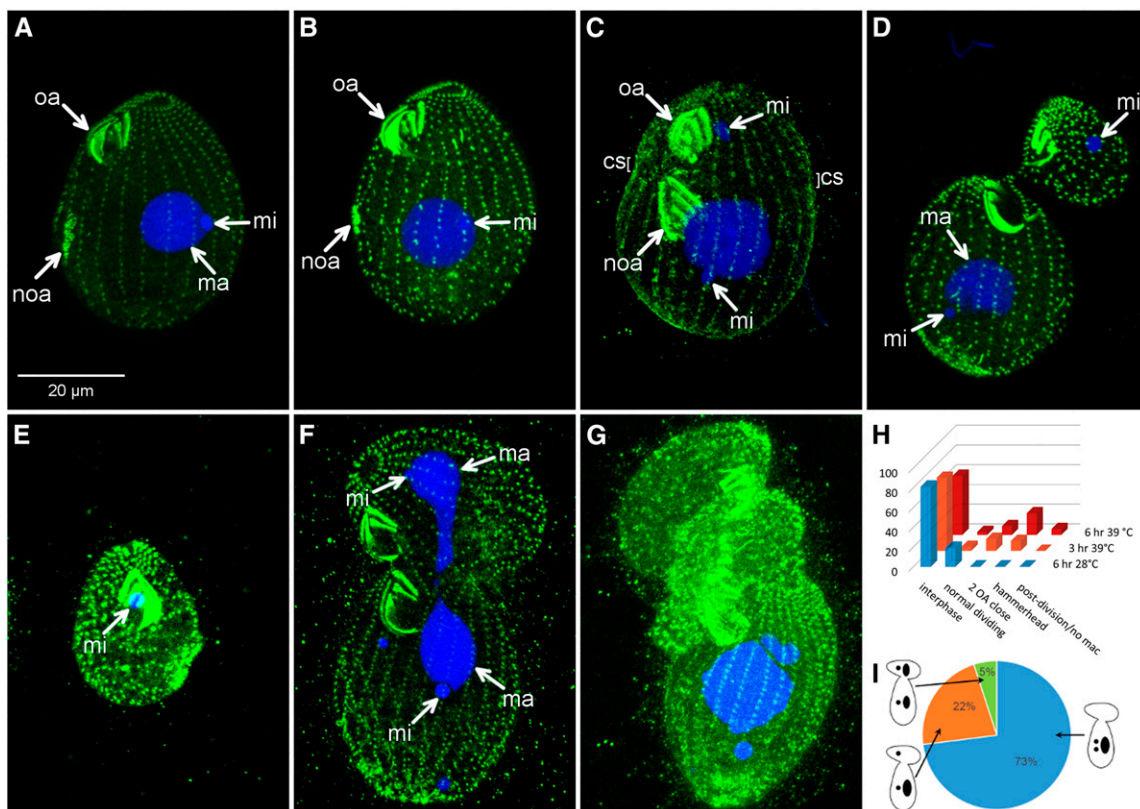


**Figure 3** The course of cortical and nuclear division in the *cda-1* *Tetrahymena* at the restrictive temperature. The *cda-1* cells were grown for 3 or 6 hr at the restrictive temperature, 39° and labeled with anti-centrin 20H5 antibodies (green) and DAPI (blue). (A, B) Mutants in an early stage of cell division, with an oral primordium (oa) present at the proper submedial position. (C) The mutant cell after the micronuclear division, with a well-developed new oral apparatus (comparable to the stage 4 in the wild type in Figure 1C). Note the anterior displacement of the new oral apparatus. The cortical subdivision is present at a proper location in relation to the new oral apparatus, and thus the entire division plane is shifted. (D) A mutant cell with a nearly completed cytokinesis. Note the failure in the division of the macronucleus resulting in its absence in the anterior daughter. (E) A cell that is an anterior product of a complete *cda-1* division, lacking a macronucleus. (F) A hammerhead cell where the anterior compartment is relatively mildly affected. Note an incomplete cortical subdivision; an asymmetry in the breakage of ciliary rows could be behind an unbalanced cortical growth that could produce the tilting of the anterior daughter. (G) A mutant cell that has produced two anterior subcells, and failed cytokinesis in two subsequent generations. (H) A diagram showing the percentages of the different morphologies observed in the *cda-1* cells at 3 and 6 hr after the temperature shift, or after 6 hr of incubation at the permissive temperature. (I) A diagram showing the percentages of nuclear end-points of cells with the hammerhead shape. oa, oral apparatus; noa, new oral apparatus; mi, micronucleus, ma, macronucleus; cs, cortical subdivision.

obtained by the same genetic scheme in non-*cda-1* backgrounds (our unpublished data), which led to 341 remaining variants. Sixty-nine of these variants were base transitions compatible with the mutagen used, nitrosoguanidine (G/C to A/T and A/T to G/C) (Ohnishi *et al.* 2008). A manual inspection of the sequence reads revealed only a single variant, scf\_8254051:142648 C to T, in the coding region of the gene *THERM\_00971920*, where 100% of sequence reads contained an alternate base (Figure 4B). In the *cda-1* pool 100% of sequence reads (28) had an alternate base, and, among them, 96% (27) contained a C to T substitution (one sequence had an A but this position was near the end of the read and thus is more likely to be a sequencing error; Mandoiu and Zelikovsky 2016). Within the wild-type pool DNA, 91% (21) of reads encoded the reference base C, and ~9% (2) had the alternate base T (Figure 4B). Since the pools of F2 clones were assembled based on their phenotypes, most likely SCGE, in addition to the expected homozygotes (Bruns *et al.* 1976) also produced some heterozygotes.

We took advantage of the recently sequenced micronuclear (germline) genome (Hamilton *et al.* 2016), to map the chromosome interval of the candidate causative mutation region in a manner similar to the approach used in other organisms including *C. elegans* (Minevich *et al.* 2012). We aligned the mutant and wild-type sequence reads to the micronuclear chromosome assembly, and determined the density of variant cosegregation with the mutant phenotype by comparing the allelic composition at variant sites between the mutant and the wild-type pool. Normalized variant cosegregation density plots revealed a single peak on the micronuclear chromosome 4, ~24 MB (Figure 4D). In the macronucleus, *THERM\_00971920* is a part of the chromosome scaffold scf\_8254051 that maps between 23.7 and 23.9 Mb on the micronuclear chromosome 4. The close match between the micronucleus-based chromosome interval mapping and the macronucleus-based variant identification achieved by subtractions and filtering, gave us confidence that we had indeed identified the causative variant.

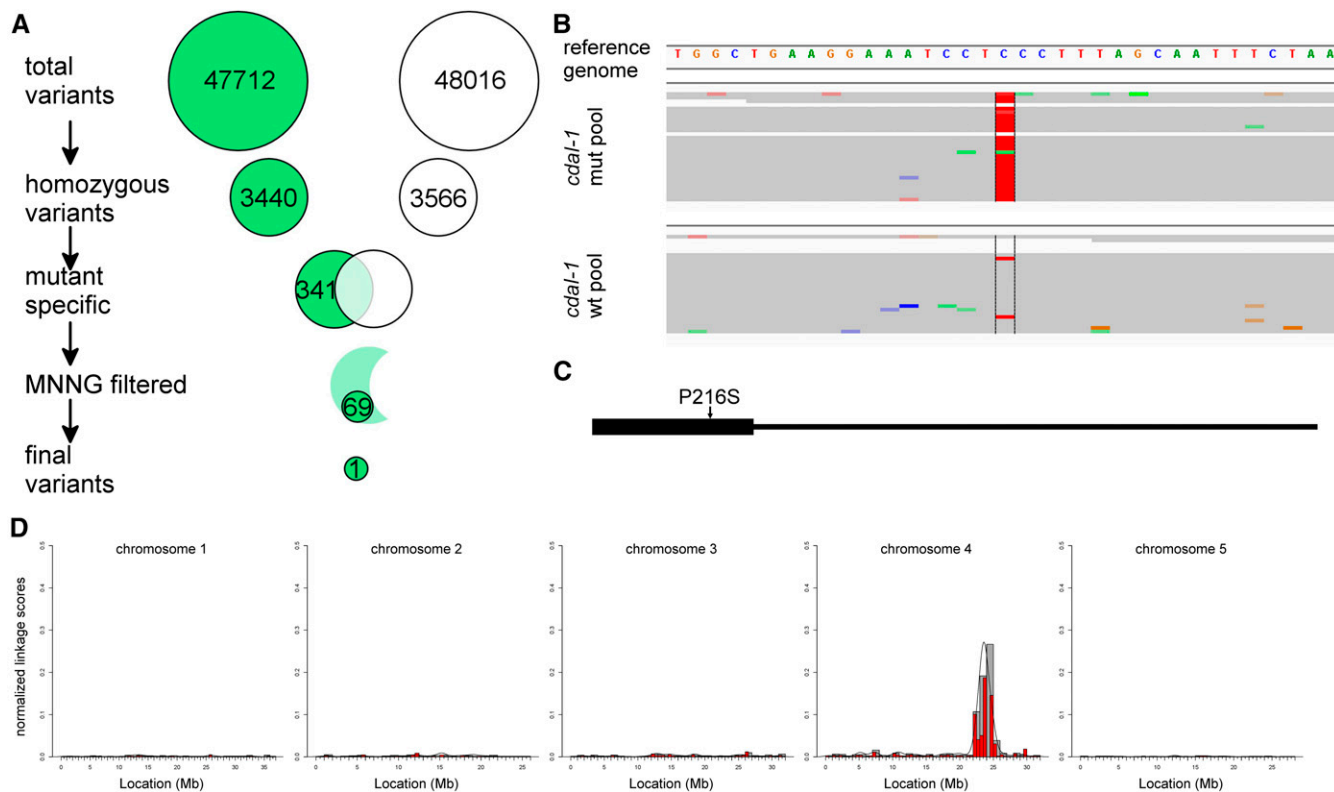


**Figure 4** Identification of the causative mutation of *cdaI-1* in *THERM\_00971920* by comparative whole genome sequencing. (A) The results of variant subtraction and filtering using macronuclear reference genome. The “MNNG filtered” step gives mutations expected for the mutagen used, nitrosoguanidine (B) Whole genome sequencing reads aligned to the region of interest in *THERM\_00971920* around the causative variant scf\_8254051:142648 (C to T) in the *cdaI-1* (top) and wild-type clonal pool (bottom). In this IGV browser view, the sequence reads are stacked underneath the reference genome sequence to which they were aligned. Reference bases are shown in gray while nonreference bases are highlighted using the same color code as in the reference genome. (C) The predicted domain organization of *THERM\_00971920* protein. The arrow shows the location of the amino acid substitution in the predicted kinase domain of *THERM\_00971920* protein. (D) Variant density mapping on the micronuclear chromosomes. Normalized linkage scores are shown along the length of each of the five micronuclear chromosomes.

The *cdaI-1* mutation is recessive (Frankel 2008). A fragment of the wild-type *THERM\_00971920* (spanning the base mutated in *cdaI-1*), when introduced by biolistic transformation into vegetative *cdaI-1* cells, produced rescue clones that divided normally at the restrictive temperature (Figure 5, A and B), while no rescues were seen in the negative control that was mock-transformed ( $n = 10^7$  cells). Sanger DNA sequencing of two rescue clone DNAs detected the mutant base (T) and the wild-type base (C) at the same position (Figure 5C and data not shown), indicating that both alleles were present in the same cells, consistent with a partial replacement of the mutant allele by a wild-type allele in the polycopy macronucleus (reviewed in Chalker 2012). Thus, we conclude that the scf\_8254051:142648 C to T mutation in *THERM\_00971920* causes *cdaI-1*.

The *THERM\_00971920* gene that we now rename *CDAI*, encodes a protein, CdaI, with a single N-terminally located kinase domain (Figure 4C). Based on reciprocal BLASTP searches, the closest homologs of the predicted CdaI protein are kinases belonging to the Hippo/Mst group, including Hippo in *Drosophila melanogaster*, MST2 in humans, and Kic1 in the budding yeast. For example, the kinase domain of CdaI is 47% identical (65% similar) to that of human

MST2. The scf\_8254051:142648 C to T mutation translates into a P216S substitution in CdaI, which is located within the kinase domain (Figure 4C). We used homology modeling to predict the 3D structure of the CdaI kinase domain based on the structure of human MST2 (PDB: 4LGD) (Ni *et al.* 2013) (Figure 5D). P216 maps to the  $\alpha$ F- $\alpha$ G loop a region involved in substrate binding and protein recognition (Kannan and Neuwald 2004, 2005; Lodowski *et al.* 2006; Sours *et al.* 2008). P216S is predicted to impact substrate binding by altering the conformation of the  $\alpha$ F- $\alpha$ G loop (Figure 5D). It is also possible that the mutant S216 serves as a gained phosphorylation site (Radivojac *et al.* 2008) that alters the activity or substrate specificity of CdaI.

#### ***CdaI* is expressed in a highly polarized pattern during cell division**

To localize CdaI protein within the cell, we tagged the ORF of *CDAI* by adding a GFP-encoding sequence at the 3' end, so that the gene product is expressed under its own promoter. We could not detect CdaI-GFP in nondividing cells (Figure 6A). In cells approaching cell division that started to develop an oral primordium, CdaI-GFP was present as lines of dots and dashes that corresponded to the ciliary rows, but the

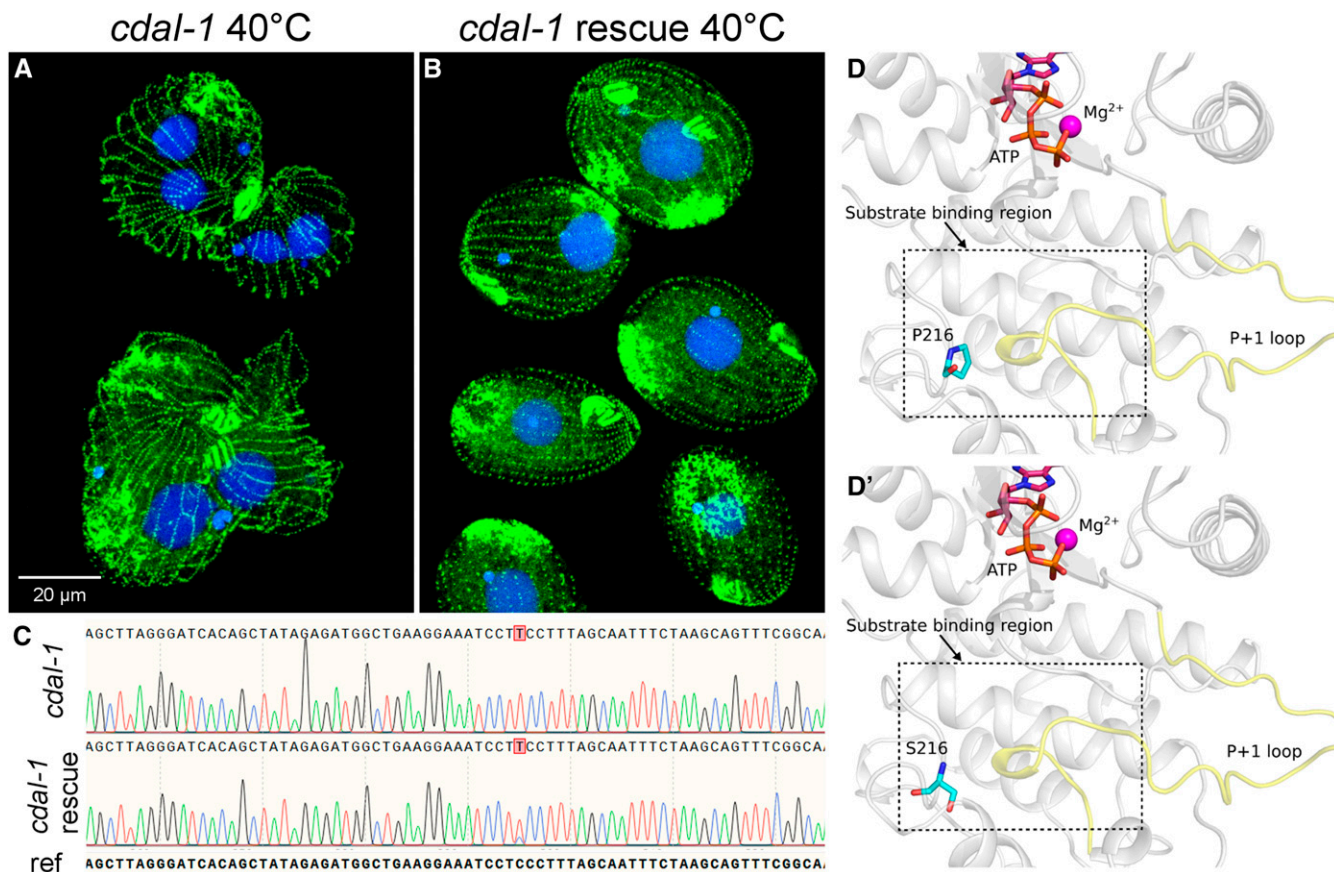


**Figure 5** A wild-type *THERM\_00971920* fragment spanning codon 216 complements *cdal-1*. The P216S mutation affects the kinase domain. (A, B) *cdal-1* cells (A) and *cdal-1* cells rescued by biolistic transformation with a wild-type *THERM\_00971920* fragment (B), were grown overnight at the restrictive temperature and stained with anti-centrin (green) and DAPI (blue). (C) Sanger DNA sequencing chromatograms showing the region of interest within *THERM\_00971920* ORF (with the mutation site shown in a red box) in the original *cdal-1* mutant and a rescue clone. Note the presence of the reference C along with the alternate T base at the position of scf\_8254051:142648 in the rescue clone. (D, D') Modeled 3D structure of the kinase domain of CdaI in its wild-type (D) and *cdal-1* (P216S) mutant version (D').

signal was much stronger in the anterior half of the cell that gives rise to the future anterior daughter (Figure 6, B–D). At this stage, most cells had a uniform circumferential pattern of CdaI-GFP (Figure 6D), while in some the signal was stronger on the ventral side, above the oral primordium (Figure 6, B and C). When the cortical subdivision appeared (staged by the completed micronuclear mitosis), the signal of CdaI-GFP was enhanced as a circumferential band of short ribbons above the division plane (Figure 6E). The oral apparatuses, both old and new, also appeared positive for CdaI-GFP (Figure 6E), but the background fluorescence tends to be higher in these locations (Figure 6, I and J). During early cytokinesis/macronuclear division, CdaI-GFP remained strong on the anterior side of the fission zone (Figure 6F). At this stage, CdaI-GFP also marked the new contractile vacuole pores (CVPs) that assemble on the right side of the cell near the posterior end of the emerging anterior daughter (Figure 6G, arrows). When the constriction zone became narrow, the CdaI-GFP signal was present at the posterior end of the emerging anterior daughter cell (Figure 6H).

The appearance of the CdaI-GFP signal coincides with the onset of cortical subdivision and the subsequent cytokinesis.

To examine in detail the relationship between CdaI and cortical morphogenesis, we labeled the CdaI-GFP-expressing cells with anti-centrin to detect the basal bodies (Figure 7, green) and anti-GFP antibodies (red) to detect the cortical CdaI. Cortical CdaI-GFP first appeared in the anterior half of the dividing cell in the early stage of the oral primordium development (Figure 7, A and A'). CdaI-GFP became prominent and uniform along all ciliary rows of the anterior subcell when the oral primordium was advanced to the stage of individualization of the oral rows, but before the cortical subdivision (Figure 7, B and B'). Thus, it appears that the establishment of the posterior edge of the CdaI-GFP lines does not require a cortical subdivision. The CdaI-GFP lines were composed of dots that roughly corresponded to the basal bodies, as well as dashes that were located between or on the side of the basal bodies (Figure 7, B and B', inset). When the cortical subdivision appeared, CdaI-GFP lines polarized by increasing in intensity near the anterior side the cortical subdivision, but a weaker signal was still present across and below the cortical subdivision (Figure 7, C and C'). When the division plane started to constrict, the CdaI-GFP signal was limited to the anterior side of the cortical subdivision; CdaI-GFP was also present between the

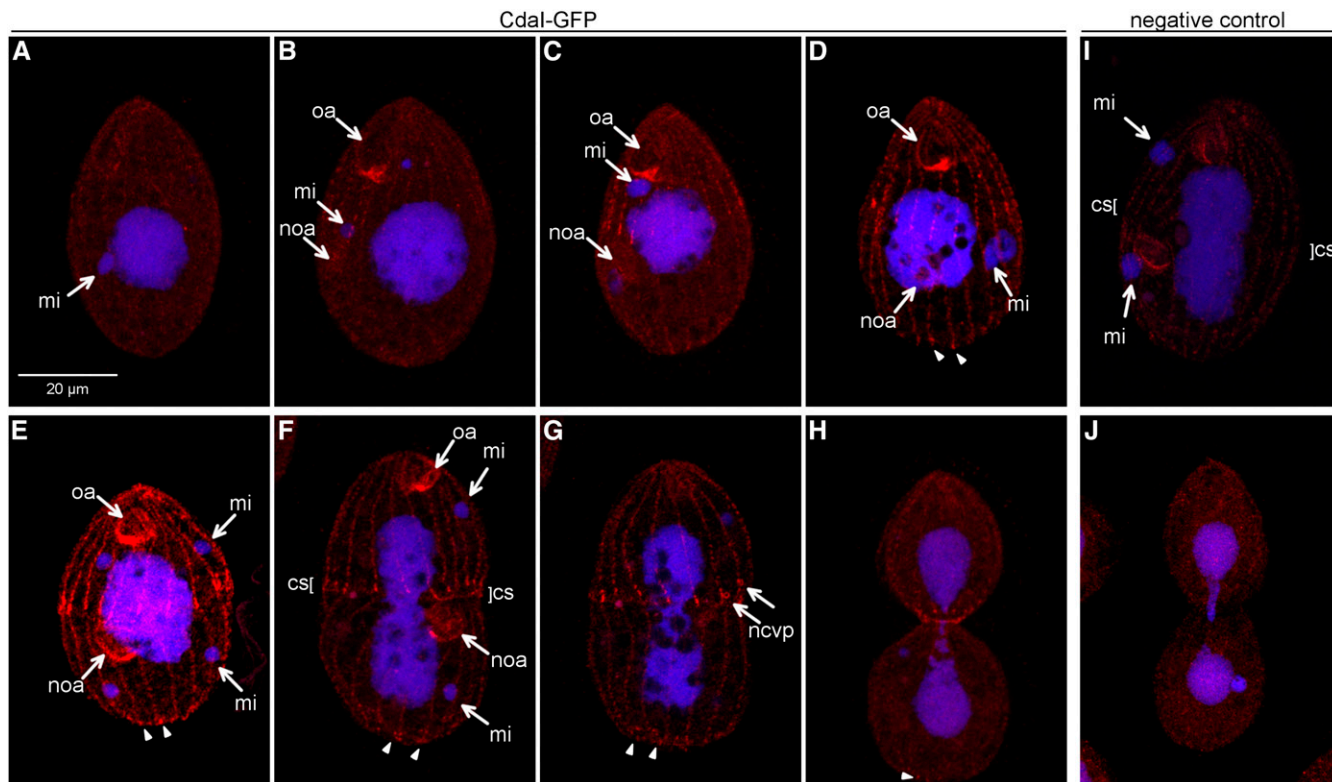


**Figure 6** CdaI is a cortical protein with a polarized and cell cycle-dependent localization and strong association with the division plane. (A–H) Cells that express CdaI-GFP but are otherwise wild-type, were labeled by immunofluorescence with anti-GFP antibodies (red) and costained with DAPI (blue). (A) An interphase cell; note the absence of a CdaI-GFP signal above the background [compare to the negative controls in (I) and (J)]. (B, C) Cells in early cell division with a young oral primordium still lacking well differentiated oral rows (the primordium can be seen based on the background staining). In addition to the anterior subcell bias, CdaI appears stronger along a few ventral rows above the oral primordium especially in the cell shown in (B). (D) A cell in an early stage of cortical subdivision (judging by the well-developed oral primordium and the micronucleus in anaphase). CdaI-GFP is strong and uniform along all of the ciliary rows of the anterior subcell. (E) A cell with a more advanced cortical subdivision based on the completed mitosis of the micronucleus (this cell has two micronuclei, both have divided, this and other nuclear abnormalities are not uncommon in transgenic strains that are selected with paromomycin). Note the enhancement of CdaI-GFP immediately anterior to the cortical subdivision in the form of short ribbons. (F, G) The same cell in early cytokinesis and early amitosis shown on two sides. Note focusing of CdaI-GFP signal along the posterior border of the anterior subcell. In (G) new CVPs are positive for CdaI-GFP (arrows). (H) A cell in late cytokinesis and late amitosis. The CdaI signal is present mainly at the posterior end of the anterior daughter. (I, J) Negative control (wild-type) cells lacking the CdaI-GFP transgene and labeled in the same way as the CdaI-GFP expressing cells shown in (A–H). mi, micronucleus; cs, cortical subdivision; ncvp, new CVPs; oa, oral apparatus; noa, new oral apparatus. In (D–H) the arrowheads point at the speckles of CdaI-GFP at the extreme posterior end of the cell that likely correspond to the preexisting Mob1 (see Figure 1 and Discussion).

neighboring ciliary rows along the constriction plane (Figure 7, D and D' inset, also see Figure 6F). During more advanced cytokinesis, CdaI-GFP was concentrated along the portions of the ciliary rows near the posterior end of the anterior subcell (Figure 7, E and E').

#### ***elo1-1* shifts both the division plane and the posterior boundary of CdaI**

To explore how the CdaI localization is influenced by the cell division events, we analyzed the pattern of CdaI-GFP in another cell division mutant, *elo1-1*, in which the division plane is dramatically shifted to the posterior cell pole (Frankel 2008). In *elo1-1*, the division plane is shifted already at the stage of the early oral primordium, the first sign of cell division (Figure 8, A–B'). Despite the posterior shift, the course of cell division in *elo1-1* cell appeared normal except for twisting of ciliary rows that was apparent at cytokinesis (Figure 8, A–D). In the *elo1-1* background, the pattern of

CdaI-GFP lines conformed to the new position of the division plane but was otherwise normal. On the ventral side, the posterior edge of the CdaI-GFP lines reached the top of the oral primordium. Strikingly, on the dorsal side, the ends of CdaI-GFP lines were at normal equatorial positions, while on the cell's sides, these ends were intermediate in their anteroposterior positions (Figure 8, B–D). This creates a remarkable slant in the position of the posterior boundary of the CdaI lines (Figure 8, B–D) as compared to an equatorial placement of the CdaI edge in the wild type (Figure 7, B–D). This indicates that Elo1 acts primarily within the oral circumferential sector. Thus, the CdaI pattern is influenced by earlier cell division events that position the division plane, and the *ELO1* gene product is probably upstream of CdaI. We also note that, in addition to the signal of CdaI-GFP within the anterior subcell, there was a consistent signal near the posterior (old) cell's end, especially in *elo1-1* cells with a cortical subdivision (Figure 8, C–E', arrowheads). A reexamination of

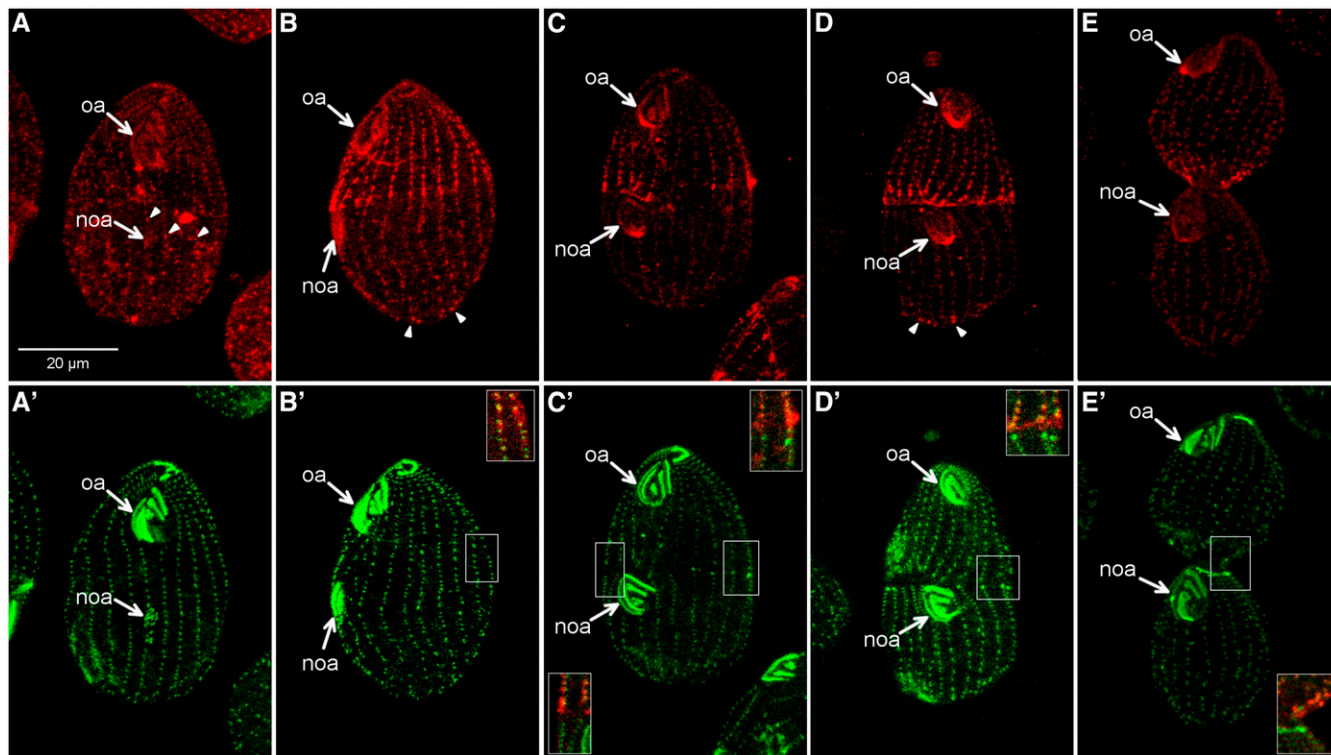


**Figure 7** The CdaI pattern changes during cortical subdivision and cytokinesis. Cells expressing CdaI-GFP (otherwise wild type) were labeled with anti-GFP antibodies (red, A–E), and anti-centrin (green, A'–E'). Insets show merged images of magnified fragments. (A–B') Cells in an early stage of cell division with a young oral primordium, with the cell in (A) and (A') in an earlier stage as compared to the cell in (B) and (B'). In (A) and (A') a very weak cortical CdaI-GFP is present in the anterior cell's half. Arrowheads show the posterior ends of the lines of CdaI-GFP. (C and C') A cell in an early stage of cortical subdivision. Note the presence of the CdaI-GFP mostly on the anterior side of the cortical subdivision (see insets). (D and D') A cell in early cytokinesis. CdaI-GFP marks strongly the posterior ends of the ciliary rows (of the anterior subcell) and interconnects the rows above the cortical subdivision. (E and E') A cell in advanced cytokinesis. CdaI-GFP marks the posterior ends of ciliary rows of the anterior subcell. In (B) and (D), the arrowheads mark the speckles of CdaI-GFP at the extreme posterior end that likely correspond to the preexisting Mob1 (see Figure 1 and Discussion). oa, old oral apparatus; noa, new oral apparatus.

wild-type cells also revealed weak foci of CdaI-GFP near the posterior cell's end (Figure 6, D–H and Figure 7, B and D, arrowheads) that appeared specific as they were not seen in the negative controls (Figure 6, I and J). The extreme posterior CdaI-GFP may represent a pool of CdaI that interacts with its likely substrate, Mob1, that was deposited in the previous cell cycle (see Discussion).

#### ***cdal-1* does not abolish the correct placement of the posterior end organelles**

Since CdaI eventually becomes focused on the posterior end of the anterior subcell, we explored whether its deficiency affects the patterning of the new CVPs that form near the new posterior end (see Figure 1). CVPs contain microtubules that are enriched in acetyl-K40  $\alpha$ -tubulin (Gaertig *et al.* 1995), which can be detected with the 6-11 B-1 antibody (Piperno and Fuller 1985). In the *cdal-1* cells grown at the permissive temperature, we detected the CVPs at proper posterior locations in 97% of interphase cells ( $n = 73$ ) (Figure 9, A and B). Furthermore, new CVPs were readily seen above the fission zone whenever the cortical subdivision was also present (Figure 9, C and D). To determine whether the *cdal-1* cells assemble new CVPs at the restrictive temperature, we exam-

ined cells that were the anterior products of a complete cell division but with clear signs of CdaI deficiency, based on their small size and an absence of a macronucleus. Surprisingly, in 75% ( $n = 33$ ) of those mutant anterior daughters, CVPs were present at proper posterior positions (Figure 9, G–K). The true frequency of CVPs in the anterior offspring is probably higher because some of them have disorganized ciliary rows that likely result from an incomplete cortical subdivision, making the identification of CVPs more difficult. In the hammerhead cells (many of which appear to have failed cytokinesis), CVPs were present in 61% of anterior subcells ( $n = 55$ ). However, in the CVP-positive hammerheads, the positions of CVPs within the anterior subcells were often incorrect (38%,  $n = 34$ ), with CVPs located either at the same anteroposterior level as the old oral apparatus (Figure 9, E and E'), or strikingly, above the old oral apparatus (Figure 9, F and F'). At the least, the assembly of the CVPs is less dependent on CdaI as compared to other cell cycle events such as the equatorial cortical subdivision, cytokinesis, and macronuclear division. Likely, CdaI is not required for the assembly of the CVPs; it is difficult to determine whether the abnormal placement of the new CVPs in the hammerheads is a result of the CdaI deficiency or is secondary to the variable cortical

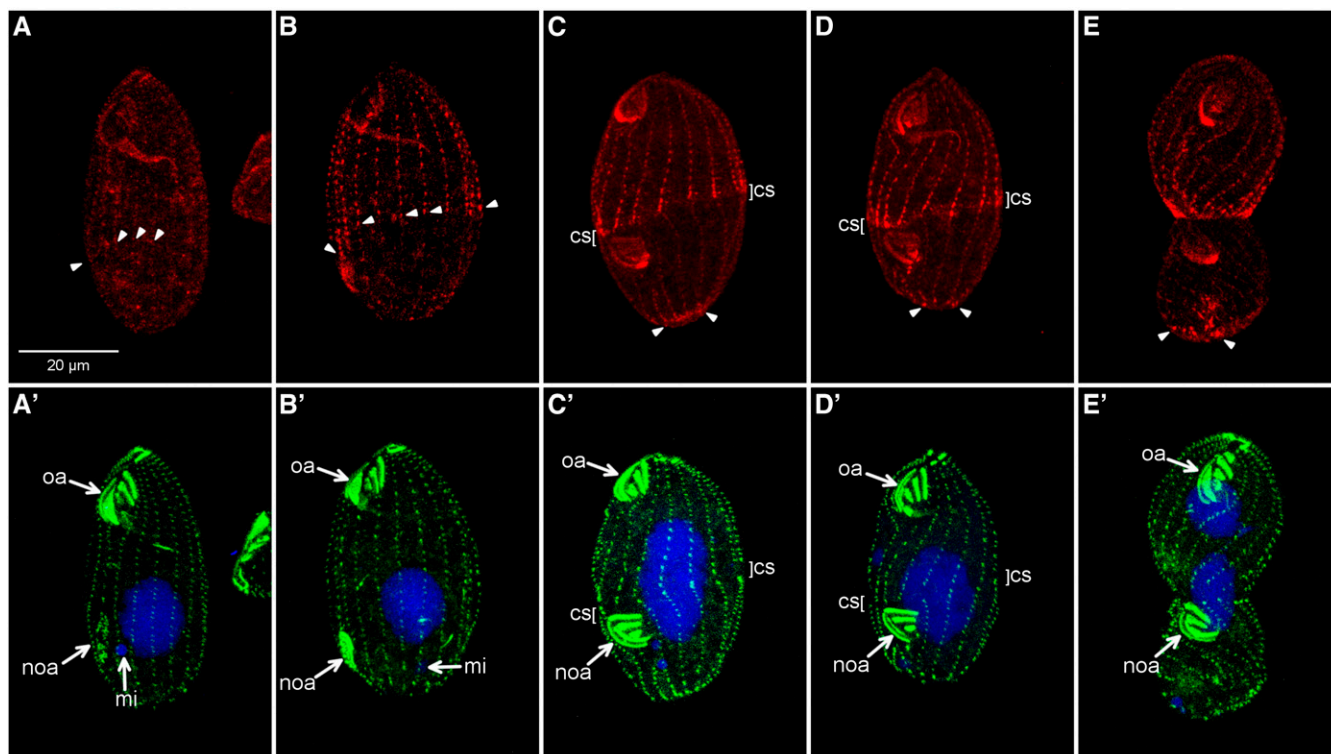


**Figure 8** The posterior boundary of CdaI is influenced by *ELO1*. CdaI was tagged with a C-terminal GFP, and expressed under the native promoter in the cell division mutant *elo1-1* (grown at the standard temperature 30° at which the mutant phenotype is expressed). Cells were labeled to detect CdaI-GFP (red in A–E), centrin (green in A'–E') and DNA with DAPI (blue in A'–E'). (A, A') A cell in an early stage of cell division. Note that the very young oral primordium assembled at an excessively posterior position. A weak signal of CdaI-GFP is present, stronger in the area immediately above the new oral apparatus. Arrowheads mark the ends of the weak CdaI-GFP lines. (B, B') A cell with a more advanced oral primordium but before the cortical subdivision. The pattern of CdaI-GFP is essentially the same as in the wild type at the similar stage (see Figure 7, B and B') except that the posterior boundary of CdaI-GFP is shifted in compliance with the more posterior position of the oral primordium. (C–D') *elo1-1* cells with a cortical subdivision. Note that the posterior shift of the edge of CdaI-GFP is prominent in the oral sector but progressively less apparent in the rows positioned away from the oral sector, and the ends of CdaI-GFP lines appear normal (equatorial) at the extreme dorsal side. This gives a slant to the edge of the CdaI-GFP lines (compare to Figure 7, C and D). (E, E') *elo1-1* mutant in cytokinesis. Note an excessively small size of the posterior daughter. In (C–E) the arrowheads point to the speckles of CdaI-GFP at the extreme posterior end that may represent CdaI-GFP bound to the old Mob1 (see Discussion). cs, cortical subdivision; oa, oral apparatus; noa, new oral apparatus; mi, micronucleus.

defects. In summary, CdaI does not seem to play a major patterning role in the assembly of at least one posterior cortical organelle, the CVP, but may have some role in limiting the placement of these organelles near the posterior cell end.

## Discussion

### The core of Hippo signaling is conserved in ciliates

The elements of the Hippo pathway that are highly conserved and essential for Hippo signaling (the Hippo core) are: (1) upstream kinase Hippo/Mst, (2) downstream kinase Warts/Lats, and (3) Warts/Lats activator Mats/Mob1 (reviewed in Hilman and Gat 2011; Sebe-Pedros *et al.* 2012; Thompson and Sahai 2015; Meng *et al.* 2016). We show that a mutation in a Hippo/Mst kinase of *Tetrahymena*, CdaI, causes an anterior migration of the division plane, and defects in cytokinesis and nuclear divisions. The Hippo/Mst kinases phosphorylate themselves, the Warts/Lats kinase, and its activator Mats/Mob1 (reviewed in Meng *et al.* 2016). All three phosphorylations are needed to produce an active tertiary complex of

Hippo/Mst-Warts/Lats-Mats/Mob1 (Gogl *et al.* 2015). Importantly, a knockdown of Mob1 in *Tetrahymena* generates a cell division phenotype that closely resembles that of *cdal-1* (Tavares *et al.* 2012), indicating that CdaI and Mob1 are in the same pathway, and that *cdal-1* is a loss-of-function mutation. Furthermore, an RNAi knockdown of Mob1 affects cytokinesis and cell shape in *Stentor* (Slabodnick *et al.* 2014). Thus, ciliates use a canonical Hippo core during cell division. The respective localizations of CdaI and Mob1 show a striking overlap, but also some informative differences. CdaI appears earlier in the cell cycle, and marks the anterior half of the cell, shortly before the cortical subdivision (Figure 1, stage 3). Mob1 appears later near the posterior boundary of CdaI (Figure 1, stage 4) (Tavares *et al.* 2012). CdaI is in the right place and time to phosphorylate Mob1, and this event could stabilize Mob1 and enable its accumulation in the fission zone. This is based on the observations in budding yeast, where the proper localization of Mob1 requires activity of a Hippo/Mst, Cdc15 (Luca *et al.* 2001) that phosphorylates a scaffolding protein, Nud1, to create a binding site for Mob1 on the spindle

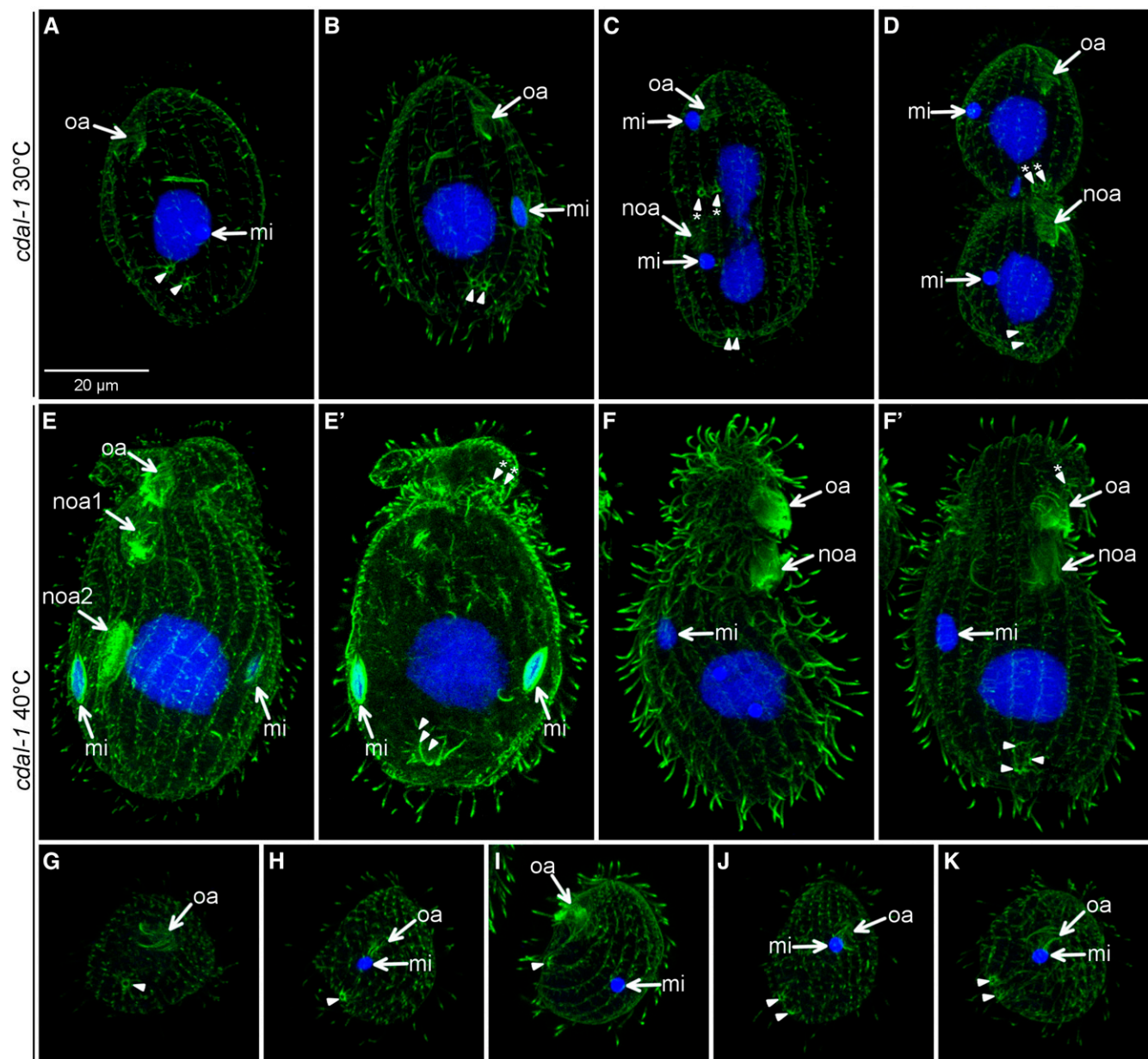


**Figure 9** New CVPs form in the anterior daughter but their locations are disturbed when cytokinesis fails due to CdaI mutation. (A–K) *cda1-1* cells grown at the permissive 30° (A–D) or restrictive (39°) temperature (E–K) for 5 hr, and labeled with 6-11 B-1 anti-acetyl-K40  $\alpha$ -tubulin (green) and DAPI (blue). Arrowheads show old CVPs and arrowheads/asterisks show new (assembling) CVPs. (A) An interphase cell. (B) A cell shortly before the cortical subdivision. Note that the old CVPs are present but the new ones that will appear along the same meridians (indicated by asterisks) are not visible yet. (C) A cell in early cytokinesis. The old and new CVPs are present. (D) A cell in late cytokinesis. The old and new CVPs are present. (E, E') The same hammerhead cell (seen on two sides) in which the posterior subcell has entered the second cell cycle (since the temperature shift) based on the presence of two micronuclei in anaphase. The anterior subcell has failed to separate and receive progeny nuclei. In the anterior subcell, a pair of new CVPs are present on the side of the old oral apparatus. (F, F') The same hammerhead cell (seen on two sides) in which the anterior subcell has failed to separate and receive a nucleus. Note a new CVP present in the anterior subcell above the old oral apparatus. (G–K) Cells that are derived from the anterior subcells of mutants that have managed to separate, despite severe defects in the nuclear divisions (lacking macronuclei). Note the presence of new CVPs at the roughly correct posterior positions.

pole body (SPB) (Rock *et al.* 2013). Interestingly, in *Tetrahymena*, the signal of CdaI around the fission zone increases at about the time when Mob1 appears (Figure 1, stage 4). There could be a positive feedback where the active CdaI-Mob1-Warts/Lats complex amplifies CdaI. Such a feedback loop operates in the fission yeast (Feoktistova *et al.* 2012).

*Tetrahymena pyriformis* cells treated with a serine-threonine kinase inhibitor, 6-dimethylaminopurine, arrest in cytokinesis, with an anteriorly displaced division plane (Kaczanowska *et al.* 1999), which is a partial phenocopy of *cda1-1*. Thus, 6-dimethylaminopurine could inhibit CdaI, or another kinase in the same pathway. The anterior cell contraction and the

hammerhead shape could be useful for high throughput screens for additional inhibitors of the Hippo pathway, which are of therapeutic interest in the context of cancer and organ regeneration (Anand *et al.* 2009; Ehmer and Sage 2016; Fan *et al.* 2016).

In other species, the Hippo components associate with the cytoskeleton, namely microtubules and microfilaments. In fungi, the Hippo pathway proteins associate with the SPBs, the contractile ring and septum (Frenz *et al.* 2000; Luca *et al.* 2001; Menssen *et al.* 2001). In *Tetrahymena*, both CdaI and Mob1 strongly accumulate along the ciliary rows, and near the microtubule-based CVPs (this study and Tavares *et al.* 2012). It should be noted, however, that cell division is almost normal in the *disA-1 Tetrahymena* mutant, in which the ciliary rows are disorganized (Jerka-Dziadosz *et al.* 1995; Galati *et al.* 2014). Thus, in *Tetrahymena*, the Hippo pathway may not require a correct pattern of cortical organelles, but it remains to be determined whether some microtubule-binding activity is important, as is the case in budding yeast (Menssen *et al.* 2001).

Another conserved property of the Hippo signaling is the asymmetry of its components. In budding yeast, during mitosis, Cdc15 initially associates with the mother (new) SPB, and later becomes enriched at the daughter (old) SPB (Menssen *et al.* 2001). In fission yeast, the Hippo/Mst kinase Cdc7 first localizes to both SPBs, but later becomes enriched at the old SPB (Sohrmann *et al.* 1998; Guertin *et al.* 2000). In *Tetrahymena*, CdaI undergoes a step-wise polarization: first it marks the anterior half of the cell, and later focuses at the posterior end of the anterior subcell. In fission yeast, time-dependent post-translational modifications have been proposed to distinguish between the old and new SPB to confer polarization of the Hippo components (Johnson *et al.* 2012). In ciliates, the new oral apparatus appears shortly before the cortical CdaI. Thus, the difference in age between the new and old oral apparatus could contribute to the subsequent asymmetry of the Hippo components. Curiously, in budding yeast, when the daughter SPB is ablated, the Hippo components become enriched on the “wrong” (mother) SPB and this reverse asymmetry is sufficient for cytokinesis (Magidson *et al.* 2006). In the light of the directional flexibility of the Hippo core observed in fungi, it perhaps is not surprising that ciliates utilize this pathway in the unique context of tandem duplication (Figure 1).

### **Hippo signaling and cytokinesis in ciliates**

The Hippo pathway is important for cytokinesis in diverse eukaryotes including fungi, protists, plants and mammals (Gromley *et al.* 2003; Yang *et al.* 2004; Citterio *et al.* 2005; Hammarton *et al.* 2005; Rohlf *et al.* 2007; Yabuta *et al.* 2007; Ma *et al.* 2010; Hergovich and Hemmings 2012; Tavares *et al.* 2012; Meitinger *et al.* 2013; Slabodnick *et al.* 2014; Bui *et al.* 2016). The *cdal-1* mutants either delay or abort cytokinesis. A stronger allele, *cdal-3*, causes an almost complete block in cytokinesis (J. Frankel, unpublished data). In fungi and animals, the Hippo signaling renders phosphorylations of the

components of the contractile ring (Yang *et al.* 2004; Meitinger *et al.* 2013). However, in ciliates the molecular mechanism of cytokinesis is divergent; ciliates do not use septins in cell division (Wloga *et al.* 2008), and the contractile ring operates without myosin-2 and conventional actin (Sugita *et al.* 2009, 2011; Shimizu *et al.* 2013). In fission yeast, overexpression of a MEN Hippo/Mst kinase, Cdc7, induces ectopic contractile rings (Fankhauser and Simanis 1994). However, in *Tetrahymena*, depletion of CdaI causes multiple defects that occur before cytokinesis (see below), or about the time of cytokinesis (and amitosis). Thus, either CdaI controls multiple subroutines in cell division including cytokinesis, or it acts at an earlier step, and affects cytokinesis as a downstream consequence.

### ***Cdal* may not play a major role in cortical patterning of the emerging daughters**

In all three of the *Tetrahymena cdaI* mutants: *cdal-1*, *cdal-2*, and *cdal-3* (Frankel 2008; this study; and J. Frankel, unpublished observations), the anterior subcell collapses after its initially correct demarcation, which is manifested by a close juxtaposition of the old oral apparatus and oral primordium. Thus, Hippo signaling may play a role in the morphogenesis of the emerging daughters. In this scenario, even the earliest phenotype of *cdal-1*, the migration of the oral primordium could be a consequence of failure in specifying the anterior compartment. Such a function would be analogous to what has been documented in budding yeast, where Hippo signaling activates transcription specifically in the daughter cell nucleus (Colman-Lerner *et al.* 2001). The main, if not only, output of CdaI activity is likely the generation of a pool of active tertiary complex with Mob1 at the new posterior end. However, we find here that the posterior end cortical markers, CVPs, assemble correctly in the *cdal-1* anterior cells that have managed to separate, despite their severe defects in nuclear division and segregation. It remains to be determined whether CdaI plays a role in other activities that take place at the new ends of emerging cortices including the remodeling of the submembranous cytoskeleton, and control of ciliation of basal bodies (Frankel *et al.* 1981; Jerka-Dziadosz 1981; Ohba *et al.* 1986; Numata *et al.* 1995; Gonda *et al.* 1999; Kaczanowska *et al.* 1999; Cole *et al.* 2008). To conclude, there is no evidence that CdaI plays a role in the organelle patterning at the posterior end of the anterior daughter, besides its role in sizing the anterior compartment by maintaining the fission zone at a proper equatorial position.

### **How is *Cdal* activated and patterned**

It is unclear how the cortical CdaI is spatially regulated and why its pattern changes as the cell division progresses. The cortical lines of CdaI appear first when cell division is already under way, after the oral primordium starts to develop. Based on the pattern of CdaI-GFP in the *elo1-1* mutant, it appears that the new oral apparatus influences the posterior boundary of CdaI cortical lines, and that this effect weakens further away from the oral sector. The posterior boundary of CdaI-GFP lines

is established before the cortical subdivision appears (Figure 7B and Figure 8B). Clearly, in addition to the *ELO1* gene product, other unknown factors pattern CdaI along the anteroposterior axis. In yeast, the Hippo/MEN pathway activity is a consequence of activation of a G protein, Tem1/Spg1, that is asymmetrically enriched on the daughter SPB (Bardin *et al.* 2000). It is unlikely, however, that the factors that pattern CdaI in ciliates originate from the mitotic spindle, or, more broadly, from the nuclei. The macronucleus divides by amitosis relatively late, at the time of cytokinesis (Williams and Williams 1976), using microtubules that lack a bipolar spindle organization (Fujiu and Numata 2000). The micronucleus divides by mitosis at about the time of initiation of cortical subdivision (Kaczanowska *et al.* 1993; Joachimiak *et al.* 2004), but this is a closed mitosis that occurs without centriolar centrosomes or a structure similar to the SPB of fungi (LaFountain and Davidson 1979, 1980). Also, there is a viable strain of *T. thermophila* that lacks a micronucleus (Kaney and Speare 1983), and other *Tetrahymena* species have lost the micronucleus during evolution (Doerder 2014). Thus, the signal that activates and spatially restricts Hippo in ciliates is unlikely to come from the nuclei. To the contrary, there is evidence of a reverse “outside to inside” signaling, in which the cortex affects the nuclei (de Terra 1973, 1975; Cohen and Beisson 1980; Gaertig and Cole 2000). Thus, the signal that activates CdaI in ciliates is likely to be intrinsic to the cortex.

#### In interphase, Mob1 may act without CdaI

In interphase, Mob1 remains associated with the posterior end of the cell (Tavares *et al.* 2012), while CdaI is not detectable (Figure 1, stages 1–3). The persistence of Mob1 at the posterior end of interphase cells was also documented in *Stentor*, using anti-Mob1 antibodies (Slabodnick *et al.* 2014). The old Mob1 pool is likely present during cell division based on the presence of foci of CdaI-GFP at the posterior end of the dividing cells (Figure 6, Figure 7, and Figure 8, arrowheads). Since the expression of CdaI appears to be limited to cell division, during interphase Mob1 may be activated by one of the three additional Hippo/Mst kinase paralogs (TTHERM\_00933100, TTHERM\_01246760 and TTHERM\_00580440). A function of Mob1 in interphase is supported by the observation that a depletion of Mob1 in *Stentor* affects the ability of this large ciliate to regenerate its body shape after surgical dissection (Slabodnick *et al.* 2014). To explore the potential interphase and early cell division functions of Mob1, it will be useful to generate a fast-acting conditional allele of Mob1; such mutations have been isolated in budding yeast (Luca and Winey 1998; Luca *et al.* 2001).

#### Conclusion

We show that *Tetrahymena* uses the conserved Hippo core to maintain equatorial cell division. Despite the unique mode of cell division by tandem duplication, in ciliates, Hippo signaling shows many conserved properties, including polarization of the signaling components across the axis of cell division.

More work is needed to determine the exact mechanism of how Hippo signaling maintains the equatorial division plane in ciliates. Finally, it is compelling that, under CdaI deficiency, the plane of cell division is initially set correctly on both the anteroposterior and circumferential axes. Thus, unknown polarity factors must act upstream of CdaI to control the positional information. Among them, the *ELO1* gene product may play a critical role in specifying the anteroposterior position of the oral apparatus.

#### Acknowledgments

We are grateful to Eileen Hamilton and Eduardo Orias (University of California Santa Barbara) and Robert Coyne and Vivek Krishnakumar (Craig J. Venter Institute) for giving us access to the assembled micronuclear genome of *T. thermophila* prior to publication. This work was supported by a bridge funding from the Office of the Vice-President for Research and the Department of Cellular Biology at the University of Georgia to J.G. Funding for N.K. from the National Science Foundation (MCB-1149106) is acknowledged. The work in the R.B. laboratory was funded by grants from Deutsche Forschungsgemeinschaft (CRC746 and CRC850) and the Excellence Initiative of the German Federal and State Governments (EXC 294). E.J. was supported by a Polish Ministry of Science and Higher Education Grant (N N303 817840). G.M. was supported by a predoctoral fellowship from the National Institutes of Health (1F31NS074841-01).

#### Literature Cited

- Afgan, E., D. Baker, M. van den Beek, D. Blankenberg, D. Bouvier *et al.*, 2016 The Galaxy platform for accessible, reproducible and collaborative biomedical analyses: 2016 update. *Nucleic Acids Res.* 44: W3–W10.
- Anand, R., J. Maksimoska, N. Pagano, E. Y. Wong, P. A. Gimotty *et al.*, 2009 Toward the development of a potent and selective organoruthenium mammalian sterile 20 kinase inhibitor. *J. Med. Chem.* 52: 1602–1611.
- Bardin, A. J., R. Visintin, and A. Amon, 2000 A mechanism for coupling exit from mitosis to partitioning of the nucleus. *Cell* 102: 21–31.
- Birkeland, S. R., N. Jin, A. C. Ozdemir, R. H. Lyons, Jr., L. S. Weisman *et al.*, 2010 Discovery of mutations in *Saccharomyces cerevisiae* by pooled linkage analysis and whole-genome sequencing. *Genetics* 186: 1127–1137.
- Blankenberg, D., A. Gordon, G. Von Kuster, N. Coraor, J. Taylor *et al.*, 2010 Manipulation of FASTQ data with Galaxy. *Bioinformatics* 26: 1783–1785.
- Bruns, P. J., and T. B. Brussard, 1974 Pair formation in *Tetrahymena pyriformis*, an inducible developmental system. *J. Exp. Zool.* 188: 337–344.
- Bruns, P. J., and D. Cassidy-Hanley, 2000 Biolistic transformation of macro- and micronuclei. *Methods Cell Biol.* 62: 501–512.
- Bruns, P. J., T. B. Brussard, and A. B. Kavka, 1976 Isolation of homozygous mutants after induced self-fertilization in *Tetrahymena*. *Proc. Natl. Acad. Sci. USA* 73: 3243–3247.
- Bui, D. A., W. Lee, A. E. White, J. W. Harper, R. C. Schackmann *et al.*, 2016 Cytokinesis involves a nontranscriptional function of the Hippo pathway effector YAP. *Sci. Signal.* 9: ra23.

- Busch, C. J., A. Vogt, and K. Mochizuki, 2010 Establishment of a Cre/loxP recombination system for N-terminal epitope tagging of genes in *Tetrahymena*. *BMC Microbiol.* 10: 191.
- Chalker, D. L., 2012 Transformation and strain engineering of *Tetrahymena*. *Methods Cell Biol.* 109: 327–345.
- Cingolani, P., V. M. Patel, M. Coon, T. Nguyen, S. J. Land *et al.*, 2012 Using *Drosophila melanogaster* as a model for genotoxic chemical mutational studies with a new program, SnpSift. *Front. Genet.* 3: 35.
- Citterio, S., E. Albertini, S. Varotto, E. Feltrin, M. Soattin *et al.*, 2005 Alfalfa Mob 1-like genes are expressed in reproductive organs during meiosis and gametogenesis. *Plant Mol. Biol.* 58: 789–807.
- Cohen, J., and J. Beisson, 1980 Genetic analysis of the relationships between the cell surface and the nuclei in *Paramecium tetraurella*. *Genetics* 95: 797–818.
- Cole, E. S., P. C. Anderson, R. B. Fulton, M. E. Majerus, M. G. Rooney *et al.*, 2008 A proteomics approach to cloning fenestrin from the nuclear exchange junction of *Tetrahymena*. *J. Eukaryot. Microbiol.* 55: 245–256.
- Colman-Lerner, A., T. E. Chin, and R. Brent, 2001 Yeast Cbk1 and Mob2 activate daughter-specific genetic programs to induce asymmetric cell fates. *Cell* 107: 739–750.
- Dave, D., D. Wloga, and J. Gaertig, 2009 Manipulating ciliary protein-encoding genes in *Tetrahymena thermophila*. *Methods Cell Biol.* 93: 1–20.
- de Terra, N., 1973 Further evidence for cortical control over replication of the macronucleus and basal bodies of *Stentor*. *Dev. Biol.* 32: 313–316.
- de Terra, N., 1975 Evidence for cell surface control of macronuclear DNA synthesis in *Stentor*. *Nature* 258: 300–303.
- DePristo, M. A., E. Banks, R. Poplin, K. V. Garimella, J. R. Maguire *et al.*, 2011 A framework for variation discovery and genotyping using next-generation DNA sequencing data. *Nat. Genet.* 43: 491–498.
- Doerder, F. P., 2014 Abandoning sex: multiple origins of asexuality in the ciliate *Tetrahymena*. *BMC Evol. Biol.* 14: 112.
- Ehmer, U., and J. Sage, 2016 Control of proliferation and cancer growth by the Hippo signaling pathway. *Mol. Cancer Res.* 14: 127–140.
- Eisen, J. A., R. S. Coyne, M. Wu, D. Wu, M. Thiagarajan *et al.*, 2006 Macronuclear genome sequence of the ciliate *Tetrahymena thermophila*, a model eukaryote. *PLoS Biol.* 4: e286.
- Fan, F., Z. He, L. L. Kong, Q. Chen, Q. Yuan *et al.*, 2016 Pharmacological targeting of kinases MST1 and MST2 augments tissue repair and regeneration. *Sci. Transl. Med.* 8: 352ra108.
- Fankhauser, C., and V. Simanis, 1994 The cdc7 protein kinase is a dosage dependent regulator of septum formation in fission yeast. *EMBO J.* 13: 3011–3019.
- Feoktistova, A., J. Morrell-Falvey, J. S. Chen, N. S. Singh, M. K. Balasubramanian *et al.*, 2012 The fission yeast septation initiation network (SIN) kinase, Sid2, is required for SIN asymmetry and regulates the SIN scaffold, Cdc11. *Mol. Biol. Cell* 23: 1636–1645.
- Frankel, J., 2008 What do genic mutations tell us about the structural patterning of a complex single-celled organism? *Eukaryot. Cell* 7: 1617–1639.
- Frankel, J., L. M. Jenkins, F. P. Doerder, and E. M. Nelsen, 1976 Mutations affecting cell division in *Tetrahymena pyriformis*. I. Selection and genetic analysis. *Genetics* 83: 489–506.
- Frankel, J., E. M. Nelsen, and L. M. Jenkins, 1977 Mutations affecting cell division in *Tetrahymena pyriformis*, syngen 1. II. Phenotypes of single and double homozygotes. *Dev. Biol.* 58: 255–275.
- Frankel, J., E. M. Nelsen, and L. M. Jenkins, 1981 Development of the ciliature of *Tetrahymena thermophila*. II. Spatial subdivision prior to cytokinesis. *Dev. Biol.* 88: 39–54.
- Frenz, L. M., S. E. Lee, D. Fesquet, and L. H. Johnston, 2000 The budding yeast Dbf2 protein kinase localises to the centrosome and moves to the bud neck in late mitosis. *J. Cell Sci.* 113: 3399–3408.
- Fujiu, K., and O. Numata, 2000 Reorganization of microtubules in the amitotically dividing macronucleus of *Tetrahymena*. *Cell Motil. Cytoskeleton* 46: 17–27.
- Gaertig, J., and E. S. Cole, 2000 The role of cortical geometry in the nuclear development of *Tetrahymena thermophila*. *J. Eukaryot. Microbiol.* 47: 590–596.
- Gaertig, J., M. A. Cruz, J. Bowen, L. Gu, D. G. Pennock *et al.*, 1995 Acetylation of lysine 40 in  $\alpha$ -tubulin is not essential in *Tetrahymena thermophila*. *J. Cell Biol.* 129: 1301–1310.
- Gaertig, J., D. Wloga, K. K. Vasudevan, M. Guha, and W. L. Dentler, 2013 Discovery and functional evaluation of ciliary proteins in *Tetrahymena thermophila*, pp. 265–284 in *Cilia, Part B*, edited by W. F. Marshall. Academic Press, Cambridge.
- Galati, D. F., S. Bonney, Z. Kronenberg, C. Clarissa, M. Yandell *et al.*, 2014 DisAp-dependent striated fiber elongation is required to organize ciliary arrays. *J. Cell Biol.* 207: 705–715.
- Gogl, G., K. D. Schneider, B. J. Yeh, N. Alam, A. N. Nguyen Ba *et al.*, 2015 The structure of an NDR/LATS kinase-mob complex reveals a novel kinase-coactivator system and substrate docking mechanism. *PLoS Biol.* 13: e1002146.
- Gonda, K., K. Nishibori, H. Ohba, A. Watanabe, and O. Numata, 1999 Molecular cloning of the gene for p85 that regulates the initiation of cytokinesis in *Tetrahymena*. *Biochem. Biophys. Res. Commun.* 264: 112–118.
- Gorovsky, M. A., 1973 Macro- and micronuclei of *Tetrahymena pyriformis*: a model system for studying the structure and function of eukaryotic nuclei. *J. Protozool.* 20: 19–25.
- Gromley, A., A. Jurczyk, J. Sillibourne, E. Halilovic, M. Mogensen *et al.*, 2003 A novel human protein of the maternal centriole is required for the final stages of cytokinesis and entry into S phase. *J. Cell Biol.* 161: 535–545.
- Guertin, D. A., L. Chang, F. Irshad, K. L. Gould, and D. McCollum, 2000 The role of the Sid1p kinase and Cdc14p in regulating the onset of cytokinesis in fission yeast. *EMBO J.* 19: 1803–1815.
- Hamilton, E. P., A. Kapusta, P. E. Huvos, S. L. Bidwell, N. Zafar *et al.*, 2016 Structure of the germline genome of *Tetrahymena thermophila* and relationship to the massively rearranged somatic genome. *Elife* 5: e19090.
- Hammarton, T. C., S. G. Lillico, S. C. Welburn, and J. C. Mottram, 2005 *Trypanosoma brucei* MOB1 is required for accurate and efficient cytokinesis but not for exit from mitosis. *Mol. Microbiol.* 56: 104–116.
- Hergovich, A., and B. A. Hemmings, 2012 Hippo signalling in the G2/M cell cycle phase: lessons learned from the yeast MEN and SIN pathways. *Semin. Cell Dev. Biol.* 23: 794–802.
- Hilman, D., and U. Gat, 2011 The evolutionary history of YAP and the hippo/YAP pathway. *Mol. Biol. Evol.* 28: 2403–2417.
- Jerka-Dziadosz, M., 1981 Cytoskeleton-related structures in *Tetrahymena thermophila*: microfilaments at the apical and division-furrow rings. *J. Cell Sci.* 51: 241–253.
- Jerka-Dziadosz, M., L. M. Jenkins, E. M. Nelsen, N. E. Williams, R. Jaeckel-Williams *et al.*, 1995 Cellular polarity in ciliates: persistence of global polarity in a disorganized mutant of *Tetrahymena thermophila* that disrupts cytoskeletal organization. *Dev. Biol.* 169: 644–661.
- Joachimiak, E., J. Kaczanowska, M. Kiersnowska, and A. Kaczanowski, 2004 Syndrome of the failure to turn off mitotic activity in *Tetrahymena thermophila*: in cdaA1 phenotypes. *Acta Protozool.* 43: 291–301.
- Johnson, A. E., D. McCollum, and K. L. Gould, 2012 Polar opposites: fine-tuning cytokinesis through SIN asymmetry. *Cytoskeleton* 69: 686–699.

- Kaczanowska, J., L. Buzanska, and M. Ostrowski, 1993 Relationship between spatial pattern of basal bodies and membrane skeleton (epiplasm) during the cell cycle of *Tetrahymena*: *cdaA* mutant and anti-membrane skeleton immunostaining. *J. Eukaryot. Microbiol.* 40: 747–754.
- Kaczanowska, J., E. Joachimiak, L. Buzanska, W. Krawczynska, D. N. Wheatley *et al.*, 1999 Molecular subdivision of the cortex of dividing *Tetrahymena* is coupled with the formation of the fission zone. *Dev. Biol.* 212: 150–164.
- Kaney, A. R., and V. J. Speare, 1983 An amiconucleate mutant of *Tetrahymena thermophila*. *Exp. Cell Res.* 143: 461–467.
- Kannan, N., and A. F. Neuwald, 2004 Evolutionary constraints associated with functional specificity of the CMGC protein kinases MAPK, CDK, GSK, SRPK, DYRK, and CK2 $\alpha$ . *Protein Sci.* 13: 2059–2077.
- Kannan, N., and A. F. Neuwald, 2005 Did protein kinase regulatory mechanisms evolve through elaboration of a simple structural component? *J. Mol. Biol.* 351: 956–972.
- Kontur, C., S. Kumar, X. Lan, J. K. Pritchard, and A. P. Turkewitz, 2016 Whole genome sequencing identifies a novel factor required for secretory granule maturation in *Tetrahymena thermophila*. *G3* 6: 2505–2516.
- LaFountain, Jr., J. R., and L. A. Davidson, 1979 An analysis of spindle ultrastructure during prometaphase and metaphase of micronuclear division in *Tetrahymena*. *Chromosoma* 75: 293–308.
- LaFountain, Jr., J. R., and L. A. Davidson, 1980 An analysis of spindle ultrastructure during anaphase of micronuclear division in *Tetrahymena*. *Cell Motil.* 1: 41–61.
- Li, H., and R. Durbin, 2009 Fast and accurate short read alignment with Burrows-Wheeler transform. *Bioinformatics* 25: 1754–1760.
- Lodowski, D. T., V. M. Tesmer, J. L. Benovic, and J. J. Tesmer, 2006 The structure of G protein-coupled receptor kinase (GRK)-6 defines a second lineage of GRKs. *J. Biol. Chem.* 281: 16785–16793.
- Luca, F. C., and M. Winey, 1998 *MOB1*, an essential yeast gene required for completion of mitosis and maintenance of ploidy. *Mol. Biol. Cell* 9: 29–46.
- Luca, F. C., M. Mody, C. Kurischko, D. M. Roof, T. H. Giddings *et al.*, 2001 *Saccharomyces cerevisiae* Mob1p is required for cytokinesis and mitotic exit. *Mol. Cell Biol.* 21: 6972–6983.
- Ma, J., C. Benz, R. Grimaldi, C. Stockdale, P. Wyatt *et al.*, 2010 Nuclear DBF-2-related kinases are essential regulators of cytokinesis in bloodstream stage *Trypanosoma brucei*. *J. Biol. Chem.* 285: 15356–15368.
- Magidson, V., F. Chang, and A. Khodjakov, 2006 Regulation of cytokinesis by spindle-pole bodies. *Nat. Cell Biol.* 8: 891–893.
- Mandouiu, I., and A. Zelikovsky, 2016 *Computational Methods for Next Generation Data Analysis*. John Wiley & Sons, Hoboken, NJ.
- Marker, S., Q. Carradec, V. Tanty, O. Arnaiz, and E. Meyer, 2014 A forward genetic screen reveals essential and non-essential RNAi factors in *Paramecium tetraurelia*. *Nucleic Acids Res.* 42: 7268–7280.
- McKenna, A., M. Hanna, E. Banks, A. Sivachenko, K. Cibulskis *et al.*, 2010 The genome analysis toolkit: a MapReduce framework for analyzing next-generation DNA sequencing data. *Genome Res.* 20: 1297–1303.
- Meitinger, F., S. Palani, B. Hub, and G. Pereira, 2013 Dual function of the NDR-kinase Dbf2 in the regulation of the F-BAR protein Hof1 during cytokinesis. *Mol. Biol. Cell* 24: 1290–1304.
- Meng, Z., T. Moroiishi, and K. L. Guan, 2016 Mechanisms of Hippo pathway regulation. *Genes Dev.* 30: 1–17.
- Menssen, R., A. Neutzner, and W. Seufert, 2001 Asymmetric spindle pole localization of yeast Cdc15 kinase links mitotic exit and cytokinesis. *Curr. Biol.* 11: 345–350.
- Michelmore, R. W., I. Paran, and R. V. Kesseli, 1991 Identification of markers linked to disease-resistance genes by bulked segregant analysis: a rapid method to detect markers in specific genomic regions by using segregating populations. *Proc. Natl. Acad. Sci. USA* 88: 9828–9832.
- Minevich, G., D. S. Park, D. Blankenberg, R. J. Poole, and O. Hobert, 2012 CloudMap: a cloud-based pipeline for analysis of mutant genome sequences. *Genetics* 192: 1249–1269.
- Nelsen, E. M., J. Frankel, and E. Martel, 1981 Development of the ciliate of *Tetrahymena thermophila*. I. Temporal coordination with oral development. *Dev. Biol.* 88: 27–38.
- Ni, L., S. Li, J. Yu, J. Min, C. A. Brautigam *et al.*, 2013 Structural basis for autoactivation of human Mst2 kinase and its regulation by RASSF5. *Structure* 21: 1757–1768.
- Numata, O., H. Suzuki, H. Ohba, and Y. Watanabe, 1995 The mutant gene product of a *Tetrahymena* cell-division-arrest mutant *cdaA* is localized in the accessory zoology of specialized basal body close to the division furrow. *Zool. Sci.* 12: 133–135.
- Ohba, H., I. Ohmori, O. Numata, and Y. Watanabe, 1986 Purification and immunofluorescence localization of the mutant gene product of a *Tetrahymena cdaA1* mutant affecting cell division. *J. Biochem.* 100: 797–808.
- Ohnishi, J., H. Mizoguchi, S. Takeno, and M. Ikeda, 2008 Characterization of mutations induced by *N*-methyl-*N*-nitrosoguanidine in an industrial *Corynebacterium glutamicum* strain. *Mutat. Res.* 649: 239–244.
- Orias, E., E. P. Hamilton, and M. Flacks, 1979 Osmotic shock prevents nuclear exchange and produces whole-genome homozygotes in conjugating *Tetrahymena*. *Science* 203: 660–663.
- Orias, E., E. P. Hamilton, and J. D. Orias, 2000 *Tetrahymena* as a laboratory organism: useful strains, cell culture, and cell line maintenance. *Methods Cell Biol.* 62: 189–211.
- Piperno, G., and M. T. Fuller, 1985 Monoclonal antibodies specific for an acetylated form of  $\alpha$ -tubulin recognize the antigen in cilia and flagella from a variety of organisms. *J. Cell Biol.* 101: 2085–2094.
- Radivojac, P., P. H. Baenziger, M. G. Kann, M. E. Mort, M. W. Hahn *et al.*, 2008 Gain and loss of phosphorylation sites in human cancer. *Bioinformatics* 24: i241–i247.
- Robinson, J. T., H. Thorvaldsdottir, W. Winckler, M. Guttman, E. S. Lander *et al.*, 2011 Integrative genomics viewer. *Nat. Biotechnol.* 29: 24–26.
- Rock, J. M., D. Lim, L. Stach, R. W. Ogirodowicz, J. M. Keck *et al.*, 2013 Activation of the yeast Hippo pathway by phosphorylation-dependent assembly of signaling complexes. *Science* 340: 871–875.
- Rohlfs, M., R. Arasada, P. Batsios, J. Janzen, and M. Schleicher, 2007 The Ste20-like kinase SvkA of *Dictyostelium discoideum* is essential for late stages of cytokinesis. *J. Cell Sci.* 120: 4345–4354.
- Ruehle, M. D., E. Orias, and C. G. Pearson, 2016 *Tetrahymena* as a unicellular model eukaryote: genetic and genomic tools. *Genetics* 203: 649–665.
- Sanders, M. A., and J. L. Salisbury, 1994 Centrin plays an essential role in microtubule severing during flagellar excision in *Chlamydomonas reinhardtii*. *J. Cell Biol.* 124: 795–805.
- Sebe-Pedros, A., Y. Zheng, I. Ruiz-Trillo, and D. Pan, 2012 Premetazoan origin of the hippo signaling pathway. *Cell Rep.* 1: 13–20.
- Shimizu, Y., Y. Kushida, S. Kiriya, K. Nakano, and O. Numata, 2013 Formation and ingression of division furrow can progress under the inhibitory condition of actin polymerization in ciliate *Tetrahymena pyriformis*. *Zool. Sci.* 30: 1044–1049.
- Slabodnick, M. M., J. G. Ruby, J. G. Dunn, J. L. Feldman, J. L. DeRisi *et al.*, 2014 The kinase regulator Mob1 acts as a patterning protein for *Stentor* morphogenesis. *PLoS Biol.* 12: e1001861.
- Sohrmann, M., S. Schmidt, I. Hagan, and V. Simanis, 1998 Asymmetric segregation on spindle poles of the *Schizosaccharomyces pombe* septum-inducing protein kinase Cdc7p. *Genes Dev.* 12: 84–94.

- Sours, K. M., S. C. Kwok, T. Rachidi, T. Lee, A. Ring *et al.*, 2008 Hydrogen-exchange mass spectrometry reveals activation-induced changes in the conformational mobility of p38alpha MAP kinase. *J. Mol. Biol.* 379: 1075–1093.
- Sugita, M., K. Nakano, M. Sato, K. Toyooka, and O. Numata, 2009 The roles of actin cytoskeleton and microtubules for membrane recycling of a food vacuole in *Tetrahymena thermophila*. *Cell Motil. Cytoskeleton* 66: 371–377.
- Sugita, M., Y. Iwataki, K. Nakano, and O. Numata, 2011 Unique sequences and predicted functions of myosins in *Tetrahymena thermophila*. *Gene* 480: 10–20.
- Tavares, A., J. Goncalves, C. Florindo, A. A. Tavares, and H. Soares, 2012 Mob1: defining cell polarity for proper cell division. *J. Cell Sci.* 125: 516–527.
- Thompson, B. J., and E. Sahai, 2015 MST kinases in development and disease. *J. Cell Biol.* 210: 871–882.
- Thorvaldsdottir, H., J. T. Robinson, and J. P. Mesirov, 2013 Integrative genomics viewer (IGV): high-performance genomics data visualization and exploration. *Brief. Bioinform.* 14: 178–192.
- Williams, N. E., and R. J. Williams, 1976 Macronuclear division with and without microtubules in *Tetrahymena*. *J. Cell Sci.* 20: 61–67.
- Wloga, D., and J. Frankel, 2012 From molecules to morphology: cellular organization of *Tetrahymena thermophila*. *Methods Cell Biol.* 109: 83–140.
- Wloga, D., I. Strzyzewska-Jowko, J. Gaertig, and M. Jerka-Dziadosz, 2008 Septins stabilize mitochondria in *Tetrahymena thermophila*. *Eukaryot. Cell* 7: 1373–1386.
- Yabuta, N., N. Okada, A. Ito, T. Hosomi, S. Nishihara *et al.*, 2007 Lats2 is an essential mitotic regulator required for the coordination of cell division. *J. Biol. Chem.* 282: 19259–19271.
- Yang, X., K. Yu, Y. Hao, D. M. Li, R. Stewart *et al.*, 2004 LATS1 tumour suppressor affects cytokinesis by inhibiting LIMK1. *Nat. Cell Biol.* 6: 609–617.
- Yu, F. X., B. Zhao, and K. L. Guan, 2015 Hippo pathway in organ size control, tissue homeostasis, and cancer. *Cell* 163: 811–828.

Communicating editor: A. Gladfelter